Longistatin in tick saliva blocks advanced glycation end-product receptor activation

Anisuzzaman,[1] Takeshi Hatta,[1] Takeharu Miyoshi,[1] Makoto Matsubayashi,[1] M. Khyrul Islam,[2] M. Abdul Alim,[1,3] M. Abu Anas,[1] M. Mehedi Hasan,[4] Yasunobu Matsumoto,[5] Yasuhiko Yamamoto,[6] Hiroshi Yamamoto,[6] Kozo Fujisaki,[1] and Naotoshi Tsuji[1,5]

[1]Laboratory of Parasitic Diseases, National Institute of Animal Health (NIAH), National Agricultural and Food Research Organization, Tsukuba, Ibaraki, Japan. [2]Department of Veterinary Science, The University of Melbourne, Parkville, Victoria, Australia. [3]Department of Parasitology, Faculty of Veterinary Science, Bangladesh Agricultural University, Mymensingh, Bangladesh. [4]Department of Aquatic Bioscience, Graduate School of Agricultural and Life Sciences, and [5]Department of Global Agricultural Sciences, Graduate School of Agricultural and Life Sciences, The University of Tokyo, Tokyo, Japan. [6]Department of Biochemistry and Molecular Vascular Biology, Kanazawa University Graduate School of Medical Sciences, Kanazawa, Japan.

Ticks are notorious hematophagous ectoparasites and vectors of many deadly pathogens. As an effective vector, ticks must break the strong barrier provided by the skin of their host during feeding, and their saliva contains a complex mixture of bioactive molecules that paralyze host defenses. The receptor for advanced glycation end products (RAGE) mediates immune cell activation at inflammatory sites and is constitutively and highly expressed in skin. Here, we demonstrate that longistatin secreted with saliva of the tick *Haemaphysalis longicornis* binds RAGE and modulates the host immune response. Similar to other RAGE ligands, longistatin specifically bound the RAGE V domain, and stimulated cultured HUVECs adhered to a longistatin-coated surface; this binding was dramatically inhibited by soluble RAGE or RAGE siRNA. Treatment of HUVECs with longistatin prior to stimulation substantially attenuated cellular oxidative stress and prevented NF-κB translocation, thereby reducing adhesion molecule and cytokine production. Recombinant longistatin inhibited RAGE-mediated migration of mouse peritoneal resident cells (mPRCs) and ameliorated inflammation in mouse footpad edema and pneumonia models. Importantly, tick bite upregulated RAGE ligands in skin, and endogenous longistatin attenuated RAGE-mediated inflammation during tick feeding. Our results suggest that longistatin is a RAGE antagonist that suppresses tick bite–associated inflammation, allowing successful blood-meal acquisition from hosts.

Introduction

Ticks are notorious blood-sucking ectoparasites, and about 1,000 tick species are distributed throughout the world. They have immense vector potential and serve as a unique vector of various deadly diseases, such as Lyme disease, tick-borne encephalitis, Rocky Mountain spotted fever, severe fever with thrombocytopenia syndrome (SFTS), babesiosis, theileriosis, and anaplasmosis (1–3). While feeding on a single blood meal, ticks remain attached to hosts, firmly embedding their barbed mouthparts for several days. Unlike some hematophagous insects, ticks cannot cannulate individual blood vessels; instead, they lacerate tissues and vascular beds with their specialized mouth parts and establish a feeding lesion in the skin, popularly known as a blood pool, from which they feed on blood and exudates until repletion. Grossly, the affected areas become purple to dark red depending on the feeding phase. Neighboring blood vessels become prominent and congested. Blood pools contain copious amounts of unclotted blood and exudates, especially at the rapid phase of feeding. A considerable amount of blood oozes out when an engorging tick is forcefully removed. Histologically, in primary infestation, the blood pool is flooded with rbc, making a clear hemorrhagic zone. There are diffuse accumulations of inflammatory cells, mostly at the periphery of the blood pool. In subsequent infestations, the blood pool is relatively inconspicuous, and dermal accumulation of inflammatory cells is markedly increased. In both secondary and tertiary infestations, the feeding success of ticks is drastically reduced and some ticks are found to die in situ. Observations reveal that the development of a blood pool is a prerequisite to the feeding biology of ticks. Extensive tissue damage and development of a blood pool are common features in tick feeding (4, 5). In fact, a blood pool can be regarded as a common niche in which a highly organized molecular interaction takes place among host, vector, and invading pathogen, and each axis wants to win to survive. Vectors and pathogens try to establish successful parasitism, while in contrast, hosts want to expel them.

During evolution, multicellular organisms have developed an impressive arsenal of defenses to counteract threats from invading infections and damaging trauma. Such responses begin with the detection of potential life-threatening danger signals, such as pathogen-associated molecular patterns (PAMPs), released by attacking pathogens, and/or damage-associated molecular patterns (DAMPs/alarmins), the endogenous innate danger molecules actively secreted or passively released by dead or devitalized tissues during infection or sterile tissue damage (6–9). PAMPs, for example, lipopolysaccharide, lipoteichoic acid, peptidoglycan, bacterial DNA, viral DNA/RNA, and mannans, are mainly recognized by TLRs, retinoid acid–inducible gene I–like (RIG I-like) receptors (RLRs), AIM2-like receptors (ALRs), and nucleotide-binding oligomerization domain–like (NOD-like) receptors (NLRs), leading to inflammatory responses (7). On the other hand, DAMPs/alarmins

Conflict of interest: The authors have declared that no conflict of interest exists.
Submitted: January 10, 2014; **Accepted:** July 31, 2014.
Reference information: *J Clin Invest*. 2014;124(10):4429–4444. doi:10.1172/JCI74917.

include high-mobility group box 1 protein (HMGB1), S100 small Ca^{2+}–binding proteins and heat-shock proteins, most of which are chiefly recognized by the prototypic DAMP receptor, receptor for advanced glycation end products (RAGE). RAGE is a transmembrane, multiligand receptor belonging to the immunoglobulin super family (10). Full-length RAGE (flRAGE) is 404-aa long, consisting of a V domain (aa 23–116) followed by 2 C domains (C1, aa 124–221, and C2, aa 227–317), a transmembrane domain (aa 343–363), and a short cytosolic tail (aa 364–404) (7, 10, 11). RAGE is highly expressed during embryonic development. In adult tissues, it is constitutively expressed at high levels in skin and lungs, but at low levels in other normal tissues, including on cells involved in the innate immune system, for example, neutrophils, macrophages, monocytes, eosinophils, basophils, dendritic cells, lymphocytes, and endothelial cells (7, 12–14). However, its expression increases at the site of inflammation or where its ligands are accumulated. RAGE/ligand interaction initiates sustained cellular activation through receptor-dependent signaling involving the transcription factor NF-κB and proinflammatory cytokine production, leading to leukocyte recruitment and subsequent initiation of inflammation in different pathological settings (7, 15, 16). Owing to severe tissue damage, it is quite reasonable that tick biting, at least at the site of attachment, causes the release of DAMPs from the devitalized tissues and is most likely to be responsible for igniting inflammatory responses, which tend to prevent the damaging activities of ticks. However, ticks can cleverly manage the host responses developed against the biting insult to ensure a sufficient blood meal. Ticks' salivary gland molecules are thought to have pivotal roles in the successful feeding on blood meals from hosts (17–19).

Recently, we isolated and identified longistatin, a salivary gland protein with 2 functional EF-hand Ca^{2+}-binding motifs, from the tick *Haemaphysalis longicornis* (20), a common vector of many bacterial, viral, protozoan, and rickettsial diseases of both medical and veterinary importance, which is widely distributed in many countries, from the Far East to Australia (1, 3). Longistatin, a 15.5-kDa soluble protein, is secreted and injected into the host's tissues through saliva during the acquisition of blood meals. Longistatin degrades fibrinogen and activates plasminogen, and has been shown to be very closely linked with the blood-feeding processes of ticks. In our previous communications, we have also shown that, at the biting site of longistatin-knockdown ticks, there was massive infiltration of inflammatory cells (4, 21), indicating that longistatin is capable of modulating inflammatory responses of hosts. However, in our previous work, the mechanism by which longistatin prevents inflammatory responses of hosts during biting of ticks was not clearly understood. Therefore, in the present study, we sought to find out the underlying mechanism by which longistatin modulates immune responses of hosts. Since longistatin contains 2 Ca^{2+}-binding motifs and most of the small Ca^{2+}-binding proteins (e.g., S100 proteins) interact with pattern-recognition receptors (PRRs), especially with RAGE, and also occasionally with TLRs (22, 23), we attempted to study the interaction of longistatin with RAGE and extracellular TLRs. Here, we demonstrate that longistatin acts as an antagonist to RAGE and prevents NF-κB translocation, subsequently downregulating adhesion molecules and thus counteracting the inflammatory responses elicited during tick bites. To our knowledge, longistatin is the first RAGE antagonist identified from a disease vector.

Results

Longistatin binds with V domain of RAGE in a Ca^{2+}-dependent manner. To study the RAGE-binding ability of longistatin, purified, recombinant longistatin (rlongistatin, 0–384 nM) was reacted with immobilized commercially available RAGE. Our study revealed that rlongistatin, but not BSA, bound with RAGE in a concentration-dependent manner (Figure 1A). Next, we conducted binding assays between immobilized longistatin (4 μg/ml) and various amounts of RAGE or TLR4 (0–5 μg/ml). We found that RAGE, but not TLR4, bound with longistatin in a concentration-dependent manner, confirming an interaction between longistatin and RAGE (Figure 1B). Additionally, longistatin was also reacted with lysozyme using the same experimental settings, but we could not detect any binding (data not shown). Antibodies raised against longistatin or extracellular domains of RAGE also abolished the interaction between longistatin and RAGE (Supplemental Figure 1; supplemental material available online with this article; doi:10.1172/JCI74917DS1). Furthermore, we compared the RAGE-binding ability of longistatin with that of other established RAGE ligands, such as N^6-(carboxymethyl) lysine–BSA (CML-BSA), glyceraldehyde-BSA (Gla-BSA), HMGB1, and S100A12. We could not find any significant difference between the RAGE-binding potential of longistatin and that of other known ligands (Supplemental Figure 2). Also, we calculated K_D value of binding between RAGE and longistatin and found that longistatin bound with RAGE at an estimated K_D of 72 ± 8 nM (Figure 1A), indicating a very high affinity. In fact, ligands bind with RAGE at different affinities and estimated K_D value varies from lower nanomol (<100 nM) to higher micromol (10 μM), depending on the ligand ligated (22).

Of the RAGE ligand advanced glycation end products (AGE), most of the S100 proteins and HMGB1 bind only with the V domain, but S100A12 ligates with the C1 domain and S100A6 with the C1 and C2 domains (24). During our study, we also attempted to determine the domain(s) with which longistatin interacted. We found that longistatin significantly ($P < 0.05$) competed only with the V domain–interacting RAGE agonists, such as AGEs (e.g., CML-BSA, Gla-BSA) and HMGB1, but not with the C1 and C2 domain–interacting agonists, namely, S100A12 and S100A6 (Figure 1C), suggesting that longistatin also binds with the V domain. To validate our data further, we evaluated interactions between longistatin and recombinant V, C1, or C2 domains. As expected, we observed that longistatin bound with V domain, but not with C1 or C2 domain, confirming that longistatin interacts with the V domain of RAGE (Figure 1D). Here, we developed a 3D homology model of longistatin using the crystal structure of human multiple coagulation factor deficiency 2 like protein (hMCFD2), since longistatin has the highest homology with that molecule (20), as a template. For better understanding, the interaction between longistatin and the V domain of RAGE has been demonstrated by computational docking (Figure 1E). Ligands mainly interact with the V domain of RAGE (25) and induce downstream signaling; thus, we hypothesized that longistatin blocks the main RAGE/agonist axis and mitigates inflammation. Furthermore, since longistatin contains 2 canonical EF-hand Ca^{2+}-binding domains and it can bind Ca^{2+}, we next sought to determine the effect of Ca^{2+} on longistatin during RAGE binding. Interestingly, we observed that interaction between RAGE and longistatin was significantly ($P < 0.01$)

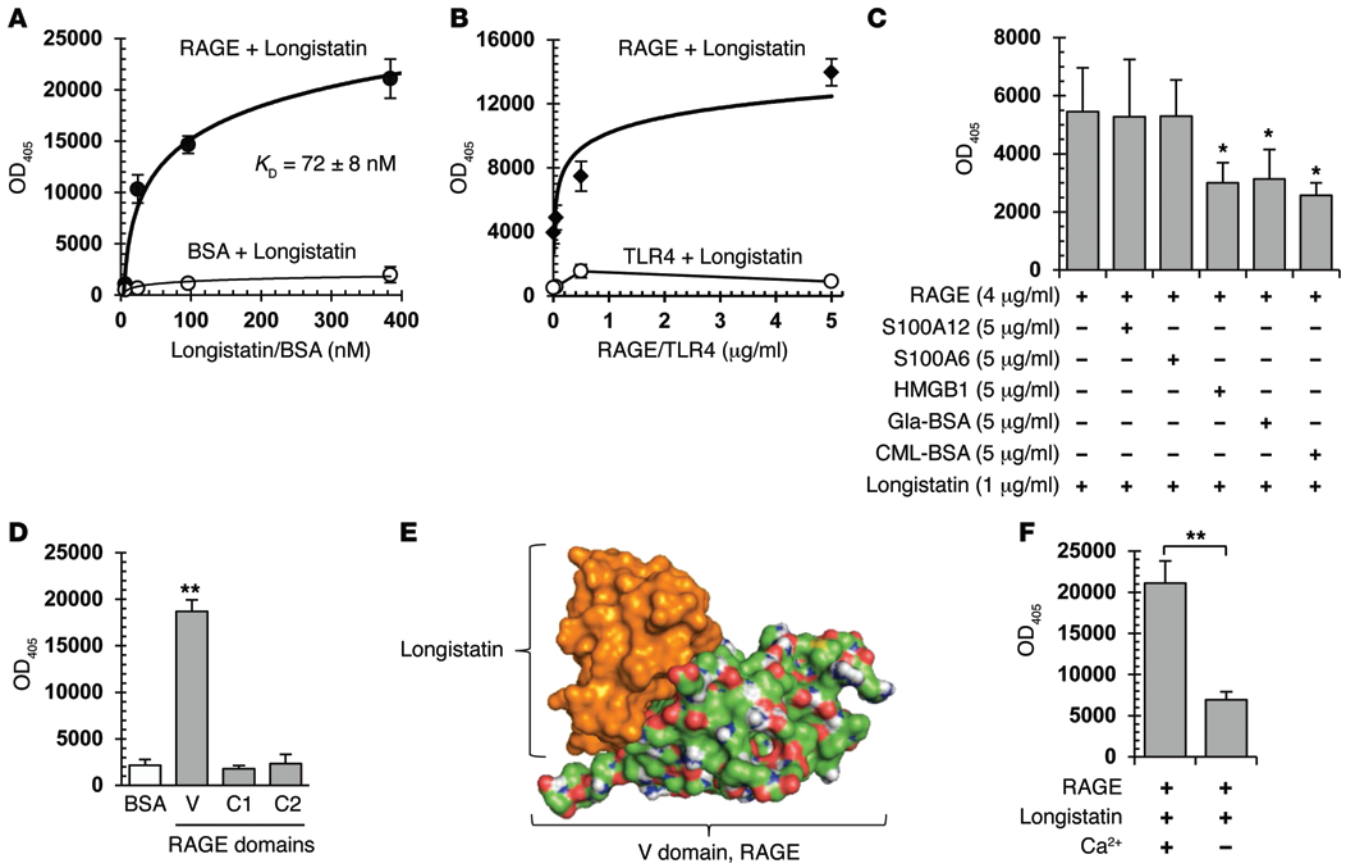

Figure 1. Longistatin binds with RAGE. (**A**) Longistatin binds with RAGE in a concentration-dependent manner. RAGE (5 μg/ml) was coated and blocked. Longistatin or BSA (0–384 nM) was added and incubated in buffer A for 1 hour at RT and treated with anti-longistatin (1:1000) or anti-BSA (1:1000) and detected with HRP-conjugated IgG. Amounts of bound longistatin were determined, and K_D value was calculated. (**B**) RAGE-dependent binding. Longistatin-coated (4 μg/ml) wells were reacted with RAGE/TLR4 (0–5 μg/ml) in 50 μl of buffer A and treated with anti-RAGE or anti-TLR4. (**C**) Competitive binding of longistatin with the V domain. RAGE (4 μg/ml) was coated, blocked, and treated with longistatin alone or with a mixture of longistatin (1 μg/ml) and each of the other RAGE ligands (5 μg/ml) as indicated, and bound longistatin was detected. (**D**) Longistatin binds with recombinant V domain. V, C1, or C2 domain (5 μg/ml) was coated and interacted with longistatin, and bound longistatin was detected. (**E**) Computational docking of longistatin to the V domain of RAGE was performed using ClusPro 2.0. (**F**) Ca^{2+}-dependent RAGE binding. RAGE-coated (5 μg/ml) wells were treated with longistatin or metal-free longistatin (6 μg/ml), and binding was detected. $n = 3$. $^*P < 0.05$; $^{**}P < 0.01$.

influenced by the presence of Ca^{2+}. The study revealed that longistatin binding was approximately 3 times higher in the presence of Ca^{2+} (Figure 1F).

Longistatin binds with the membrane-tethered RAGE. The cell surface is occupied by thousands of molecules, so the microenvironment is very complex and ligand-receptor interaction is obviously more complicated than that seen on the single-molecule–coated microtiter plates. For this reason, we planned to study the interaction of longistatin with membrane-tethered RAGE using HUVECs (Cell Application Inc.). We treated stimulated cells with longistatin followed by simultaneous treatment with anti-longistatin and anti-RAGE. During our study, longistatin-specific bright green fluorescence was detected on the HUVECs, suggesting that longistatin binds with HUVECs. Binding of longistatin was detected only in the cytoplasmic area of the cells and was almost entirely undetected in the nucleus. Also, we could detect RAGE-specific red fluorescence in the cytoplasmic area of the cells. The longistatin-specific green fluorescence and RAGE-specific red fluorescence almost completely merged (Figure 2A), suggesting that longistatin bound to HUVECs through RAGE. Additionally, using anti-RAGE and an ELISA-based microtiter plate binding assay, we also found that RAGE antigen present in the HUVEC whole-cell lysate bound with the immobilized longistatin. Detection of RAGE-specific antigen bound to longistatin directly corresponded to the concentration of anti-RAGE (Figure 2B). In addition, using anti-longistatin, we detected that longistatin binding was significantly ($P < 0.01$) higher with the membrane fractions of the stimulated cells (Supplemental Figure 3). Furthermore, we conducted pull-down assay using Talon resin–trapped (Clontech Laboratories Inc.) His-tagged longistatin and the membrane fraction of HUVECs. Eluted proteins were analyzed by Western blotting (WB) using anti-longistatin or anti-RAGE. The study revealed that longistatin coeluted with RAGE, and the complex was detected with both anti-RAGE and anti-longistatin (Figure 2C). Importantly, during pull-down assay, only one complex was detected with anti-longistatin that exactly corresponded to the band detected with anti-RAGE, suggesting that longistatin forms a stable complex only with RAGE, but not with other membrane-spanning receptors or proteins. This finding also suggests strong and stable binding between longistatin and RAGE that can withstand the effects of reducing agents present in the SDS-PAGE sample buf-

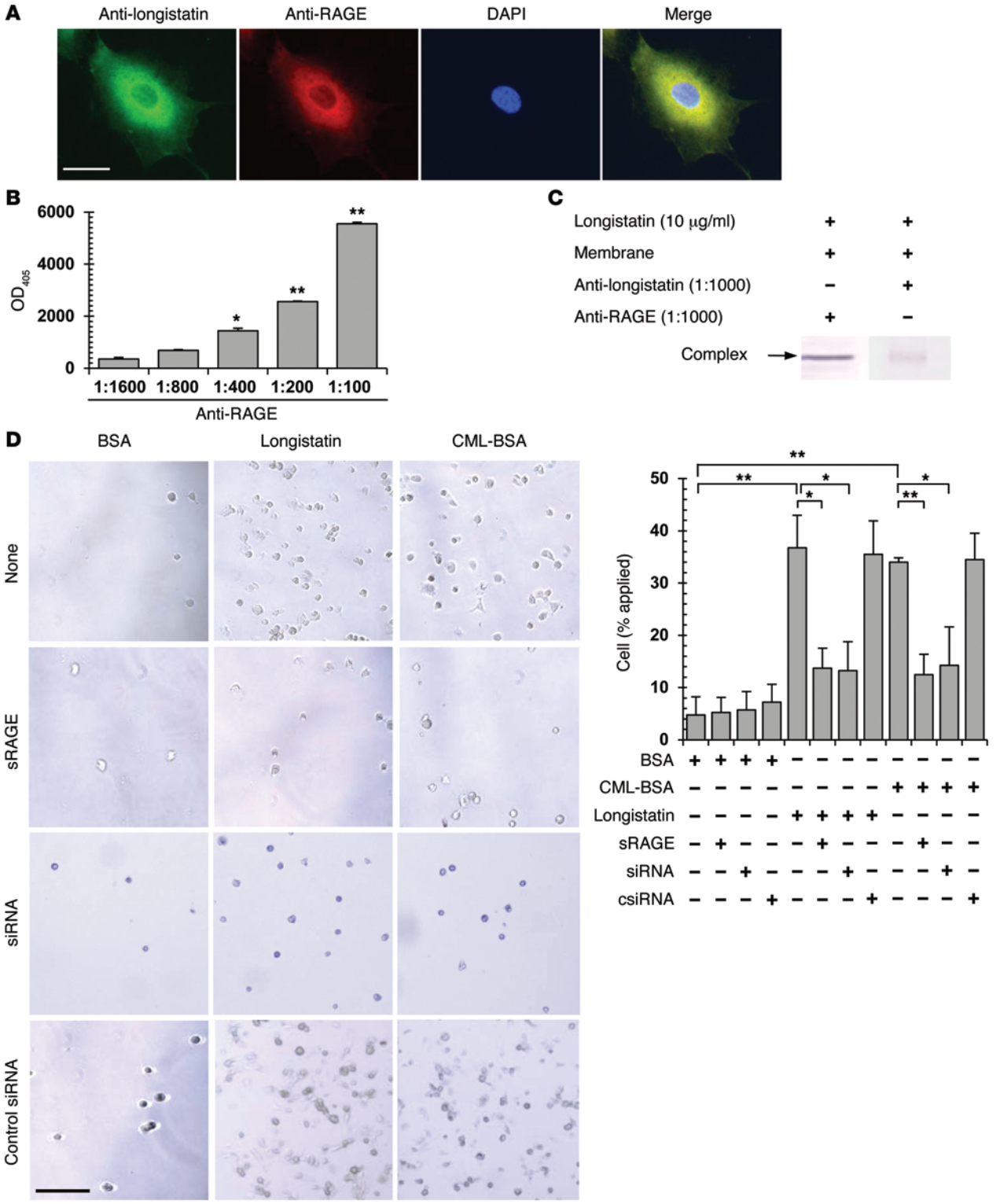

Figure 2. Longistatin binds with the membrane of HUVECs through RAGE. (**A**) Colocalization of longistatin and RAGE. Serum-starved cells were stimulated with TNF-α (1 ng/ml), fixed, and treated with longistatin (5 μg/ml), followed by the treatment with anti-longistatin (1:1000) and anti-RAGE (1:1000). Bound antibodies were probed, and images were merged. Scale bar: 20 μm. (**B**) Binding of longistatin with RAGE present in HUVEC lysate. Longistatin (5 μg/ml) was coated and reacted with whole-cell lysate. Bound protein was detected with anti-RAGE (1:1600 to 1:100). (**C**) Pull-down analysis. His-tagged longistatin (10 μg) was trapped with Talon Metal Affinity Resin and incubated with the membrane fraction of HUVECs (100 μg) in buffer A. Proteins were eluted and analyzed by WB using anti-longistatin (1:1000) or anti-RAGE (1:1000). (**D**) Ex vivo binding of HUVECs with longistatin through RAGE. Ninety-six–well cell-culture plates were coated with BSA, longistatin, or CML-BSA (5 μg/ml) and treated without or with sRAGE (5 μg/ml) for 1 hour at RT. Then stimulated normal or siRNA-treated HUVECs (2×10^3 cells/well) were seeded and incubated for 2 hours, and adhered cells were counted. Scale bar: 100 μm. $n = 4$. $^*P < 0.05$; $^{**}P < 0.01$.

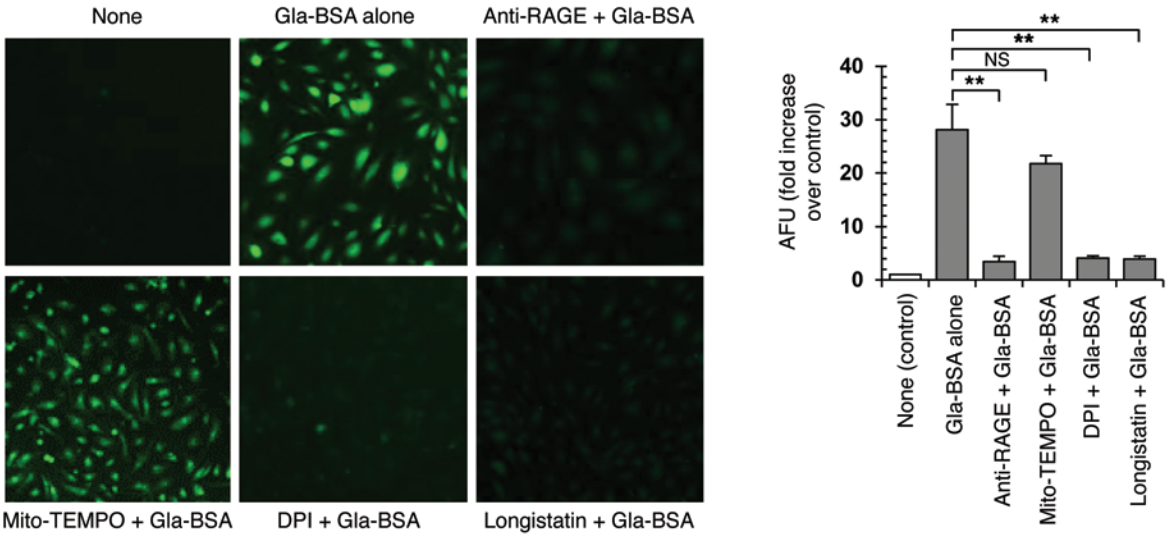

Figure 3. Effects of longistatin on cellular ROS. HUVECs (1×10^5 cells/chamber) were seeded onto chamber slides or 96-well cell-culture plates and allowed to adhere overnight. Cells were treated without or with Gla-BSA (100 μg/ml) in the absence or presence of pretreatment with anti-RAGE (1:100), DPI (20 μM), Mito-TEMPO (10 μM), or longistatin (10 μg/ml) for 2 hours. Cellular ROS were detected with the DCFDA Cellular ROS Detection Kit. Scale bar: 100 μm. $^{**}P < 0.01$. AFU, arbitrary fluorescent unit.

fer. Most strikingly, interaction between longistatin and whole-cell lysate was concentration-dependently inhibited by a neutralizing Abs to the extracellular domains of RAGE (LSBio) (Supplemental Figure 4), confirming the ligation of longistatin with RAGE. To judge further the interaction of longistatin with the membrane-tethered RAGE, we conducted a direct ex vivo experiment using HUVECs. In the same experimental setting, we found that stimulated HUVECs adhered to the longistatin- or CML-BSA–coated wells, but not to the BSA-coated ones. Importantly, sRAGE, a soluble form of RAGE, significantly ($P < 0.01$) blocked the adherence of HUVECs to the longistatin- or CML-BSA–coated wells. sRAGE is devoid of a transmembrane domain and a cytosolic tail. sRAGE is an endogenous antagonist of flRAGE, acts as a "decoy receptor," and competes with flRAGE by scavenging the same ligands (12, 26). To increase the support for our data further, we performed siRNA-mediated knockdown of RAGE in HUVECs and conducted attachment assay. We observed that RAGE siRNA, but not scrambled siRNA, significantly reduced the number of cells adhering to the longistatin- or CML-BSA–coated wells, providing clear evidence that longistatin ligated with the membrane-tethered RAGE (Figure 2D).

Longistatin reduces cellular oxidative stress. Available literature supports that RAGE/ligand engagement induces ROS production (27). Therefore, we sought to demonstrate the effects of longistatin on the production of ROS. To do this, initially, we determined whether Gla-BSA generates ROS or not. We determined that Gla-BSA induced robust ROS production in HUVEC, which was efficiently inhibited by pretreatment of HUVECs with anti-RAGE, suggesting that Gla-BSA induced ROS production via RAGE. We also observed that ROS production was potently inhibited by diphenylene iodonium (DPI), an inhibitor of NADPH oxidase, but not by Mito-TEMPO, a mitochondria-targeted ROS antagonist, suggesting that NADPH oxidase is the major source for RAGE/ligand axis–mediated ROS production in HUVECs, conforming to the findings of Wautier et al. (27), who found that AGEs trigger ROS generation in vascular endothelium by activating NADPH oxidase. To demonstrate the effect of longistatin on cellular ROS production, we treated HUVECs with longistatin and stimulated with Gla-BSA. Interestingly, we observed that longistatin effectively attenuated cellular ROS production, which was comparable to the effects of anti-RAGE on ROS generation in HUVECs (Figure 3).

Longistatin prevents NF-κB translocation. Since longistatin competes with RAGE ligands, including various alarmins, we sought to reveal the effects of RAGE/longistatin interaction on NF-κB translocation. Immunofluorescence study using anti–NF-κB revealed that pretreatment of HUVECs with longistatin prevented translocation of NF-κB from the cytoplasm to the nucleus. NF-κB–specific bright green fluorescence was clearly detected almost entirely within the cytoplasm in longistatin-pretreated cells, which was comparable to the localizations of NF-κB in unstimulated control or anti-RAGE–pretreated plus Gla-BSA–stimulated cells. In contrast, NF-κB–specific reaction was confined entirely within the nucleus when cells were stimulated with Gla-BSA without prior longistatin or anti-RAGE treatment (Figure 4A). Furthermore, we compared the relative amounts of NF-κB in the cytoplasmic and nuclear fractions of HUVECs isolated from different treatment groups. By an ELISA-based study, we detected a significantly higher level of NF-κB–specific antigen in the cytoplasmic fraction of longistatin-treated plus Gla-BSA–stimulated cells than that detected in the nuclear fraction of the same treatment group, which was comparable to the level of NF-κB detected in the different fractions of the control cells. On the other hand, a higher level of NF-κB was detected in the nucleus than in the cytoplasm of Gla-BSA–stimulated cells (Figure 4B). To temper our assertion that longistatin prevented NF-κB translocation, we performed WB using cytoplasmic and nuclear fractions. A prominent NF-κB–specific band was detected in the cytosol of the longistatin-treated plus Gla-BSA–stimulated as well as untreated or anti-RAGE–pretreated control cells. However, NF-κB was not detectable in the

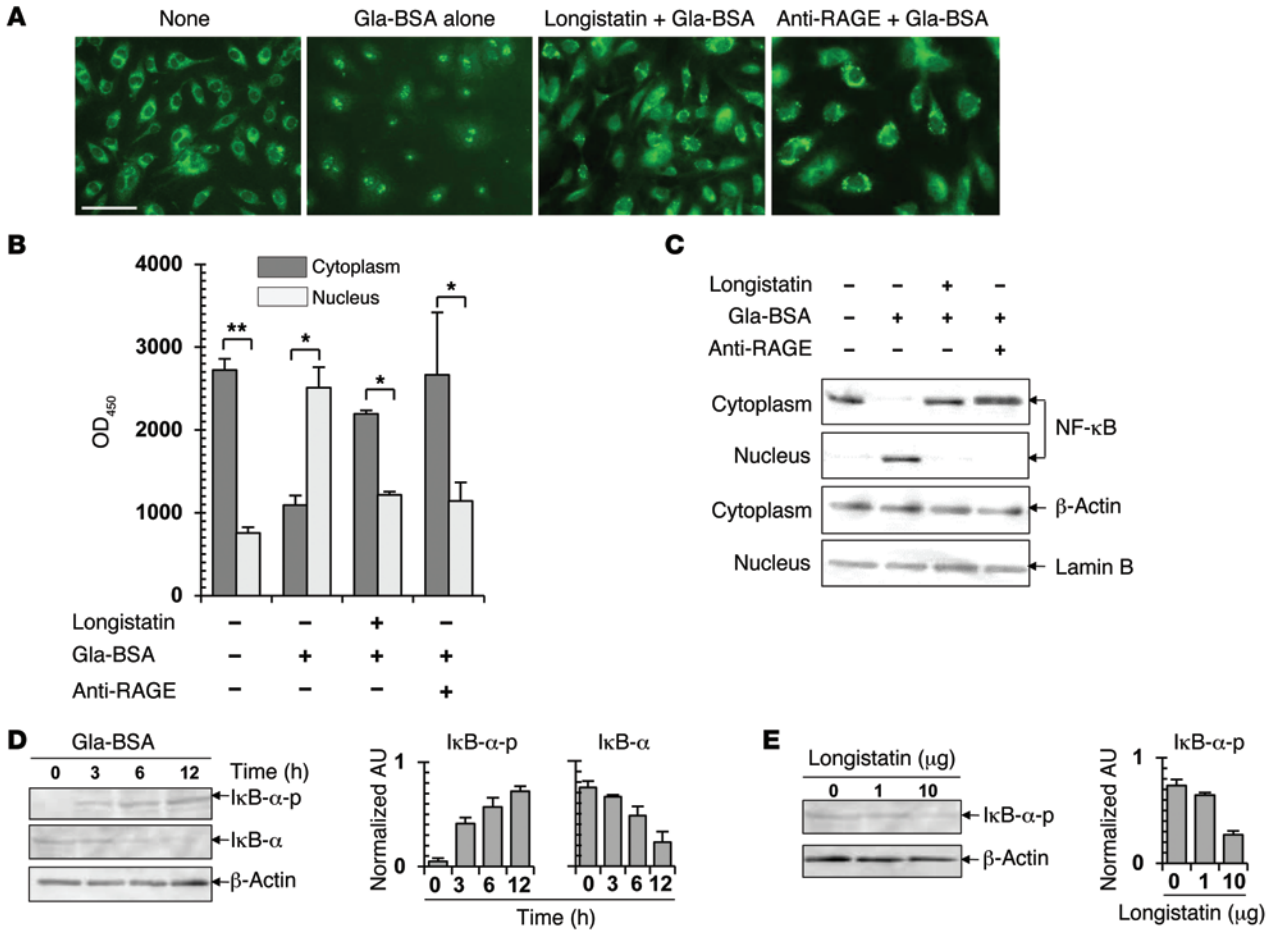

Figure 4. Longistatin prevents nuclear translocation of NF-κB. (**A**) In situ detection of NF-κB. HUVECs were grown on chamber slides and stimulated. Cells were treated with anti–NF-κB (1:1000) and a green fluorescent-labeled secondary Ab. Scale bar: 50 μm. (**B**) Detection of NF-κB in different cellular fractions. Cytoplasmic and nuclear fractions were collected, and NF-κB was determined by ELISA. (**C**) NF-κB present in the cytosolic or nuclear fraction of different treatment groups was determined by WB. (**D**) Time-dependent phosphorylation and degradation of IκB-α. Equal amounts (30 μg) of cytosolic protein from different treatment groups were separated by SDS-PAGE, and WB was performed using antibodies against IκB-α, phospho–IκB-α, or β-actin. (**E**) Inhibition of phosphorylation of IκB-α by longistatin. HUVECs were cultured, treated with longistatin (0–10 μg/ml), and stimulated with Gla-BSA, cytosol was harvested, and phospho–IκB-α was detected by WB. $^{**}P < 0.01$; $^{*}P < 0.05$.

cytoplasmic fraction of cells stimulated with Gla-BSA only. In contrast, an NF-κB–specific distinct and prominent band was detected in the nuclear fraction of Gla-BSA–stimulated cells, but neither in the nuclear fraction of longistatin-pretreated cells nor in that of control (untreated or anti-RAGE pretreated) cells, confirming that longistatin prevented the nuclear translocation of NF-κB by blocking Gla-BSA ligation with RAGE (Figure 4C). NF-κB in unstimulated cells remains sequestered in the cytoplasm by IκB. Upon stimulation, IκB undergoes phosphorylation and gradually degrades, and NF-κB becomes free and translocated into the nucleus (28). To show the effects of longistatin on NF-κB translocation, we further studied the impact of longistatin on the Gla-BSA–induced phosphorylation of IκB-α. By WB, we found that over the course of time, Gla-BSA caused gradual degradation of IκB-α with its corresponding phosphorylation (Figure 4D). Next, we pretreated HUVECs with different amounts of longistatin (0–10 μg/ml) and stimulated them with Gla-BSA. We observed that longistatin effectively prevented the phosphorylation and degradation of IκB-α (Figure 4E), further suggesting that longistatin is capable of preventing NF-κB translocation.

Longistatin suppresses expression of adhesion molecules and secretion of cytokines. A wealth of literature suggests that RAGE/ligand interaction induces upregulation of adhesion molecules (29, 30). Here, we also observed that stimulation of HUVECs with Gla-BSA sharply increased *VCAM1*, *ICAM1*, and E-selectin mRNA, which was efficiently downregulated by anti-RAGE, indicating that Gla-BSA upregulated the expression of adhesion molecules via RAGE. However, longistatin treatment prior to Gla-BSA stimulation significantly suppressed *VCAM*1, *ICAM*1, and E-selectin expression in a concentration-dependent manner, which was comparable to the effect of anti-RAGE (Figure 5A). Among the adhesion molecules, robust upregulation of *VCAM1* was detected following the RAGE ligand stimulation, which was in turn abruptly attenuated by longistatin. High expression of adhesion molecules in endothelial cells promotes interaction of circulating leukocytes with the endothelial surface, and this can eventually result in pavementation, margination, and extravasations of the reactive cells into the site of tissue injury (30). Furthermore, we also studied the effects of longistatin on the Gla-BSA–induced secretion of cytokines by HUVECs. Robust

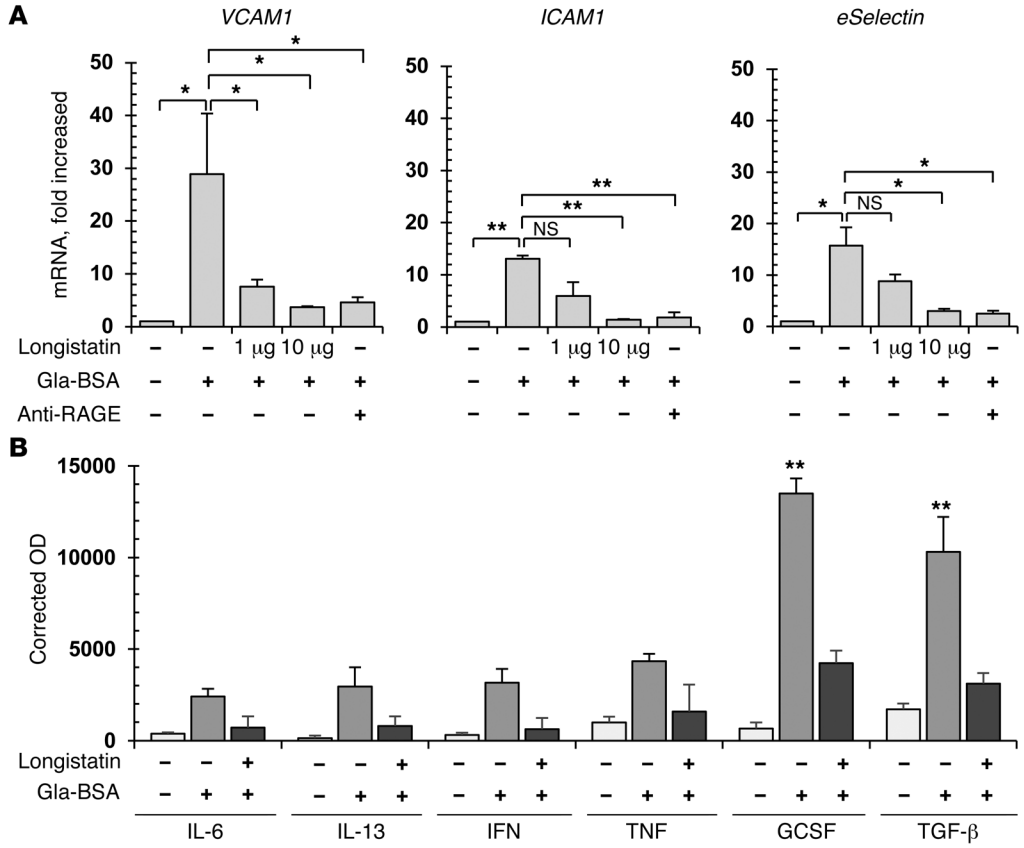

Figure 5. Longistatin reduces adhesion molecules and cytokine production. (**A**) Effects on adhesion molecule production. HUVECs were cultured and stimulated, and total RNA was collected. *VCAM1*, *ICAM1*, and E-selectin were checked by qRT-PCR using β-actin to normalize the amount of cDNA. (**B**) Effects on cytokine secretion. HUVECs were cultured and stimulated, and medium was collected. Cytokines were measured by ELISA. $n = 3$. $^{**}P < 0.01$; $^{*}P < 0.05$.

secretion of GCSF and TGF-β was detected following Gla-BSA stimulation. However, Gla-BSA treatment also slightly elevated IL-6, IL-13, IFN-γ, and TNF-α protein levels in cell-culture media. Longistatin significantly attenuated the secretion of GCSF and TGF-β into the culture media (Figure 5B).

Longistatin inhibits RAGE-mediated cell migration in vitro. Since RAGE/ligand axis–mediated cellular activation is associated with the recruitment and migration of inflammatory cells, we studied the effects of longistatin on the chemotaxis of mouse peritoneal resident cells (mPRCs). Initially, we found that Gla-BSA induced WT cells, but not RAGE-deficient cells (from mice with deletion of *Ager*, which encodes RAGE, herein referred to as $RAGE^{-/-}$), to migrate through the polycarbonate membrane of the Chemotaxicell (Kurabo Industries Ltd.) in a concentration-dependent manner (Figure 6A), suggesting clearly that Gla-BSA is capable of recruiting cells via RAGE. Next, we attempted to study the effect of longistatin on Gla-BSA–induced and RAGE-mediated cellular migrations. We observed that longistatin effectively attenuated the chemotactic responses of mPRCs toward Gla-BSA. Brief treatment of mPRCs with purified rlongistatin reduced the number of cells that migrated through the membrane of the Chemotaxicell in a concentration-dependent manner. In the absence of longistatin pretreatment, 76 ± 25 cells/focus migrated, whereas only 20 ± 9 cells/focus were found to migrate when mPRCs were pretreated with 10 μg/ml longistatin. On the other hand, 25 ± 5 cells/focus migrated when cells were pretreated with a commercially available Ab to the extracellular domains of RAGE (1:100), which was comparable to the nonspecific migration of untreated and unstimulated mPRCs toward the media alone (Figure 6B).

Longistatin prevents RAGE-mediated inflammation in mice. To prove our hypothesis, formulated from a series of in vitro and ex vivo experiments, that longistatin modulates RAGE/ligand axis–mediated cellular trafficking, we conducted a mouse footpad edema model study in WT and $RAGE^{-/-}$ mice. Initially, we studied the effect of rlongistatin on carrageenan-induced inflammation. We observed that the carrageenan-induced inflammatory phenotype was similar in WT and $RAGE^{-/-}$ mice, indicating that carrageenan-mediated inflammation was not dependent on RAGE. Importantly, we observed that longistatin did not have any significant effect on the carrageenan-induced cellular infiltration (Figure 7A), suggesting that longistatin does not modulate non–RAGE-ligand–mediated inflammation. Next, to ascertain the antiinflammatory activities of longistatin on the RAGE/ligand axis, we injected rlongistatin into the footpads of mice, followed by a single injection with Gla-BSA. Histopathological evaluation revealed that injection with Gla-BSA, without prior treatment with rlongistatin, induced massive infiltration of inflammatory cells. Pretreatment with rlongistatin efficiently reduced the number of inflammatory cells. Upon Gla-BSA injection, infiltration of inflammatory cells (301 ± 53 cells/mm^2) significantly increased compared with that in the PBS-injected footpad (75 ± 32 cells/mm^2). Mice that received rlongistatin into the footpad showed significantly fewer infiltrating inflammatory cells (152 ± 55 cells/mm^2), which were almost comparable in number to those in PBS-injected footpads (Figure 7B). Since RAGE is also constitutively and highly expressed in lung, we studied the effects of longistatin on a Gla-BSA–induced chronic pneumonia model in mice. We developed chronic pneumonia in mice by instilling Gla-BSA through the nostrils, which was

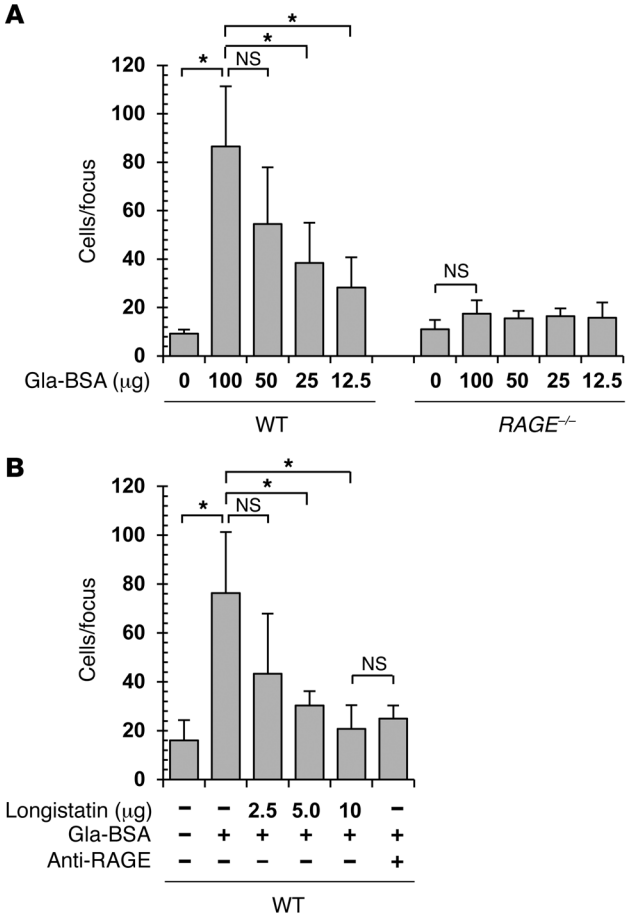

Figure 6. Effect of rlongistatin on RAGE-mediated cell migration in vitro. (**A**) Gla-BSA induced cellular migration via RAGE. mPRCs were collected from WT or RAGE$^{-/-}$ mice and seeded onto the upper chamber of Chemotaxicell in RPMI-1640 medium. The lower chamber contained RPMI-1640 medium with Gla-BSA (0–100 μg/ml) and was incubated. After gentle washing, membrane was stained with Giemsa stain, and cells were counted. (**B**) Longistatin prevented RAGE-mediated cellular migration. mPRCs from WT mice were treated with longistatin (0–10 μg/ml) or anti-RAGE (1:100) or left untreated, and chemotaxis toward Gla-BSA was determined. $n = 4$. *$P < 0.05$.

characterized by the massive infiltration of mostly mononuclear inflammatory cells. The interalveolar septa became thick, and the alveolar space became narrow, leading to the loss of normal lung architecture. Interestingly, pretreatment with longistatin efficiently prevented the Gla-BSA–induced inflammatory distortion of the lungs. Histopathological analysis revealed that pathologic changes were less severe in the lungs of the longistatin-treated mice. The lungs of mice that received longistatin showed normal parenchyma consisting of almost normal alveolar septa and alveolar spaces together with cellular components that were comparable to those in the PBS-treated mouse lungs. Cellular infiltration was significantly lower in the lungs of longistatin-pretreated groups (185 ± 30 cells/mm^2) than in the lungs of mice that received only Gla-BSA (403 ± 56 cells/mm^2) and was comparable to the level in mice that received PBS only (85 ± 14 cells/mm^2) (Figure 7C). Data obtained from our in vivo models suggest that rlongistatin prevented RAGE/ligand axis–driven inflammation in mammals.

Tick bite downregulates RAGE ligands, but not RAGE itself, during feeding on mammalian hosts. Literature available suggests that RAGE ligands are upregulated in different inflammatory diseases and conditions and that the axis plays pivotal roles in the pathogenesis of such settings (22, 23). Therefore, we sought to determine whether some RAGE ligands, especially V-domain–interacting ligands, were upregulated in the blood pool. To do this, ticks were allowed to feed on mice, and tissues from the bitten areas were collected at different feeding periods (0–120 hours). By quantitative reverse-transcriptase PCR (qRT-PCR), we could detect remarkable upregulation of *S100b*, *S100a9*, and *S100a8*. The expression of *S100b* was slightly higher (31 ± 5–fold) than that of *S100a8* (22 ± 6–fold) and *S100a9* (20 ± 10–fold). With the progress of feeding, the expression of RAGE ligands significantly increased in the blood pool. The most robust expression was detected at the peak feeding period (96–120 hours), which is known as the rapid feeding phase (Figure 8). In the rapid feeding phase, ticks cause severe tissue damage at the site of attachment on hosts (4, 5). Additionally, since RAGE also has NF-κB–binding sites and longistatin prevented NF-κB translocation, we then studied the effect of tick biting on the expression of RAGE itself. However, we observed similar patterns of RAGE expression throughout the entire feeding period of ticks, suggesting that tick bite did not significantly reduce RAGE expression in skin during feeding (Figure 8). This is possibly due to the constitutive presence of a high level of RAGE in skin.

Endogenous longistatin modulates RAGE-mediated inflammation during biting. Since we found that rlongistatin prevented inflammatory responses in mouse footpad inflammation and pneumonia models elicited by Gla-BSA, we sought to find out the effect of endogenous longistatin on affected animals directly during tick feeding processes. Using a longistatin-based RNAi technique, we found that there was massive infiltration of inflammatory cells (508 ± 20 cells/mm^2) at the attachment sites of RNAi-treated (dslongistatin injected) ticks. In contrast, at the biting area of control (*E. coli* maltose-binding protein dsRNA [ds*malE*] injected) ticks, very few inflammatory cells (141 ± 20 cells/mm^2) were detected, which is comparable to the number of reactive cells present in normal skin (feeding chamber attached but no tick bite) of mice (37 ± 20 cells/mm^2). Then, we attempted to categorize the types of cells using different special stains and/or antibodies to specific markers of various cell types. Skin section stained with direct and fast scarlet (DFS) showed that the infiltration of eosinophils (Figure 9A) was significantly ($P < 0.01$) higher at the biting site of longistatin-knockdown ticks (45 ± 8 cells/mm^2). In contrast, very few eosinophils (7 ± 3 cells/mm^2) were detected at the biting area of ds*malE*-injected ticks. We also detected a significantly higher number of anti-F4/80–specific macrophages (Figure 9A) at the biting area of longistatin-knockdown ticks. In addition, toluidine blue staining showed that the level of mast cell infiltration (Figure 9A) was a little bit higher at the biting area of RNAi-treated ticks. At the attachment site of RNAi-treated ticks, the development of a blood pool was not evident, conforming to our previous study that showed that knockdown of the longistatin gene abolishes the unique characteristics of developing blood pools (4). In contrast, blood pools were visible in the control groups; however, hemorrhagic zones in

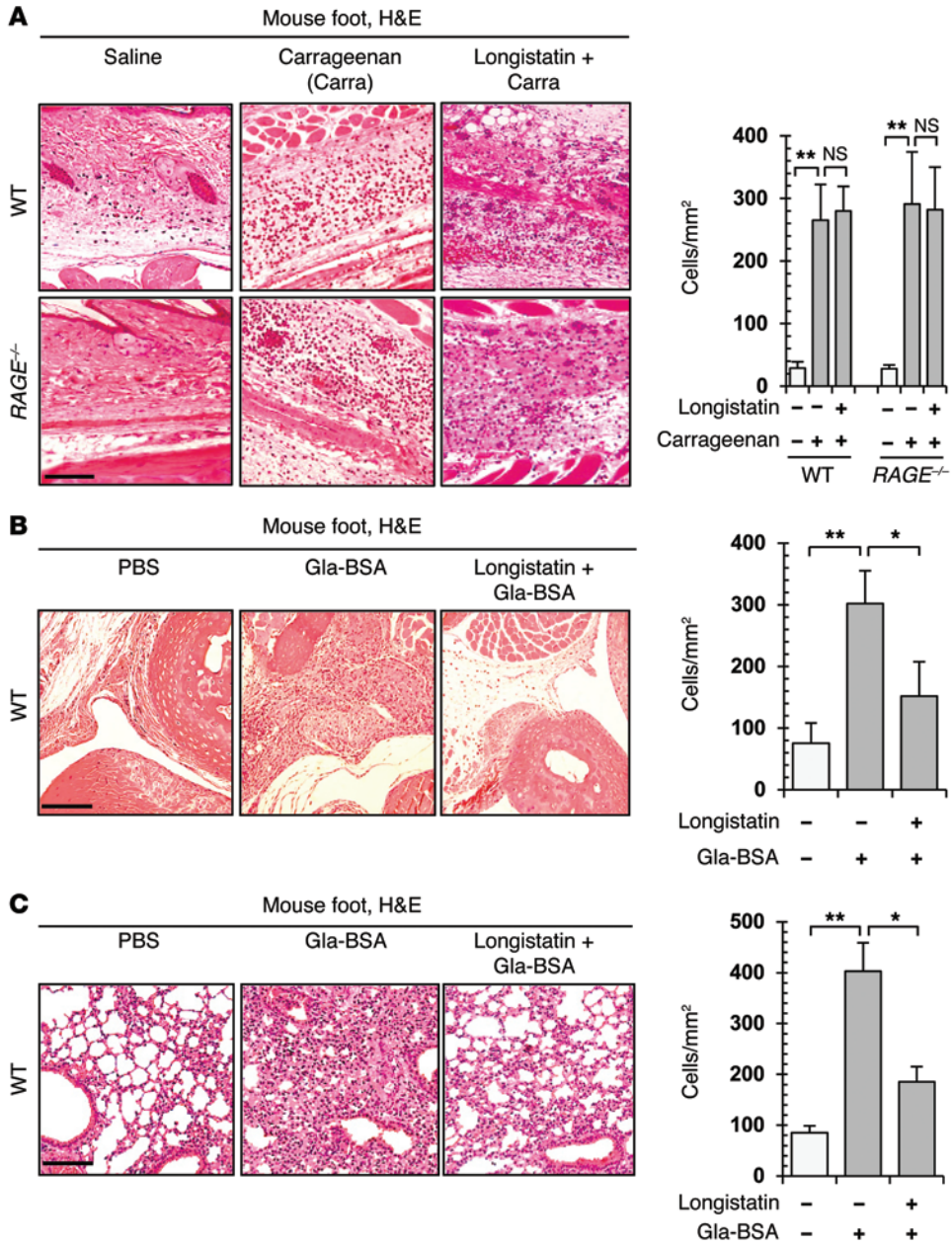

Figure 7. rlongistatin prevents RAGE/ligand-mediated inflammation. (**A**) Longistatin does not affect carrageenan-induced inflammation in WT or RAGE$^{-/-}$ mice. Longistatin (100 μg) or PBS was injected into the hind footpad of each WT or RAGE$^{-/-}$ mouse. One hour later, 2% carrageenan or saline (100 μl) was injected into the same footpad. After 5 hours, mice were euthanized and footpads were collected and fixed, and histopathological analysis was performed. Scale bar: 40 μm. (**B**) Longistatin attenuates Gla-BSA–induced mouse footpad inflammation. Longistatin (100 μg) or PBS was injected into the hind footpad of each mouse. After 1 hour, Gla-BSA (100 μg) or PBS was injected into the same footpad. Mice were euthanized at the indicated time point, and footpads were collected and subjected to histopathology. Scale bar: 40 μm. $n = 5$. (**C**) Longistatin attenuates Gla-BSA–induced pneumonia. Longistatin (50 μg) or PBS was instilled through each nostril. One hour later, Gla-BSA (50 μg) or PBS was instilled. After 48 hours, the mice were euthanized and their lungs were collected and fixed, sections were prepared and stained with H&E, and then cells were counted. Scale bar: 40 μm. $n = 6$. $^*P < 0.05$; $^{**}P < 0.01$.

the mouse back-feeding model of ticks was not as markedly evident as was detected in the rabbit ear–feeding models (4), which may be due to host species variation. It is worth mentioning that control ticks successfully became engorged on the mouse model as well. To clarify that endogenous longistatin modulated the RAGE/ligand axis of inflammation, we extended our study using WT and RAGE$^{-/-}$ mice. We attached RNAi-treated and control ticks to WT and RAGE$^{-/-}$ mice and allowed them to feed. Histological evaluation revealed that cellular infiltration was significantly higher at the areas bitten by longistatin-knockdown ticks (463 ± 44 cells/mm^2) than that detected at the areas bitten by ds*malE*-injected control ticks fed on WT mice. Importantly, cellular infiltration levels were similar at the biting areas of both the RNAi-treated and control ticks fed on RAGE$^{-/-}$ mice (Figure 9B), confirming that native longistatin, secreted and injected with tick saliva, ameliorated RAGE-mediated inflammation in hosts during tick feeding.

Longistatin modulates cytokine production during tick bite. Since we observed that endogenous longistatin efficiently downregulated eosinophil and macrophage recruitment and subsequent infiltration at the attachment site of ticks, we attempted to study relevant cytokine profiles. We measured the expression levels of different cytokines that play primary roles in regulating activation, recruitment, and functions of eosinophils and macrophages. Our qRT-PCR data showed that the expression of *Il5*, *Tnfa*, *Cox2*, and *Mcp5* significantly increased during the biting of RNAi-treated ticks. mRNA levels of *Il5*, *Tnfa*, *Cox2*, and *Mcp5* increased approximately 18-, 23-, 12-, and 16-fold, respectively, at the biting area of longistatin-knockdown ticks compared with those of normal mouse skin. In contrast, the expression of these genes was significantly lower at the attachment area of ds*malE*-injected control ticks (Figure 10A), suggesting that endogenous longistatin downregulated the expression of these genes during feeding of ticks

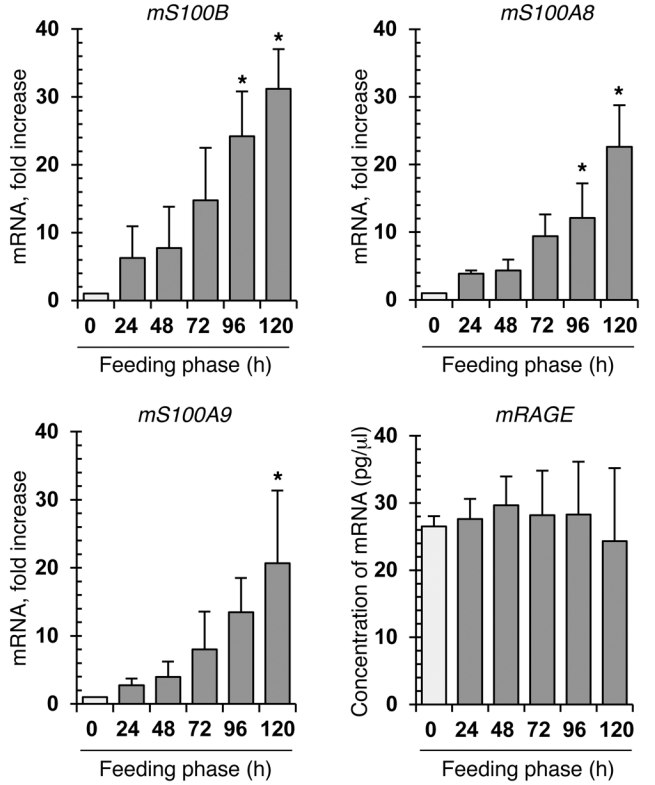

Figure 8. Expression of RAGE and RAGE ligands at the biting sites of ticks. Adult unfed ticks were allowed to feed on the shaven backs of tick-naive WT mice. Mice were euthanized at different time points (0–120 hours), and tissues were collected from the feeding lesions. Total RNA was collected, and RAGE ligands and RAGE were analyzed by qRT-PCR. $n = 5$. $^*P < 0.05$.

on hosts. Since the mRNA level of cytokines sometimes does not reflect that the cytokine is secreted, we further checked the effects of longistatin on the secretion of the cytokines by WB, and we found that the cytokines were secreted during tick bite. An equal amount of protein was loaded in each well, but we found a very prominent and distinct band of each cytokine at the biting areas of longistatin knockdown but not at the biting areas of ds*malE*-injected control ticks, further suggesting that longistatin has profound inhibitory effects on the production of these cytokines (Figure 10B).

Discussion

RAGE protein is constitutively and highly expressed in skin irrespective of age. In the skin, almost all cellular components, such as skin fibroblasts, dendrocytes, keratinocytes, endothelial cells, and mononuclear cells, express RAGE (31). Initially, it was shown that RAGE binds to AGEs, the nonenzymatically modified glycoproteins. However, a plethora of literature are now available demonstrating that RAGE can bind several classes of structurally unrelated ligands and is therefore referred to as a PRR. In fact, the receptor has the ability to recognize tertiary structures, such as β-sheets and fibrils, rather than specific aa sequences (32). In addition to AGEs, it can interact with a wide range of ligands through recognition of β-sheets and fibrillar structures of amyloid components, S100 proteins, HMGB1, Mac-1, prions, heat shock proteins (e.g., HSP70), secreted protein acidic and rich in cysteine (SPARC), complement components (e.g., C3a and C1q) and CpG-containing oligos (e.g., hCpGAs, hCpGBs, and mCpGi) (10, 13, 22, 33–35). RAGE engagement with its ligands sets up strong, sustained inflammation and plays a central role in many inflammatory diseases (14, 31, 32). Here, we show that longistatin, a secreted small EF-hand Ca^{2+}-binding protein from the tick *H. longicornis*, interacts with the V-domain of RAGE and acts as an antagonist as well as preventing inflammatory responses in hosts during tick infestation.

Through a series of in vitro experiments using purified proteins, we have clearly demonstrated that longistatin binds with RAGE. Longistatin contains 2 canonical EF-hand motifs and can bind Ca^{2+}. Previously, we showed that longistatin has pivotal effects on plasminogen-mediated fibrinolysis and blood coagulation cascades; thus, it maintains blood pool homeostasis by keeping blood in a fluid state and modulates the feeding success of vector ticks. In addition, during RNAi-mediated longistatin-knockdown study using the rabbit ear tick-feeding systems, we observed that longistatin also potently suppresses the infiltration of inflammatory cells at the feeding site of ticks (4). However, the underlying molecular mechanism of quenching inflammation by longistatin remains unclear. Our present study sheds light on the interplay between longistatin and the immune machinery that constitutively dominates in the mammalian skin. Also, we provide evidence to show that rlongistatin efficiently competes with several V-domain–interacting RAGE ligands and these ligands induce inflammation in different pathological settings, such as diabetic complications, Alzheimer disease, sepsis, psoriasis, and even tumor invasion (25, 35). Multiple effects of tick salivary gland–derived molecules (e.g., Iris) on the hosts' coagulation and inflammation have also been reported (36). Possibly, ticks gained longistatin during coevolution with their hosts to deceive the immune system of hosts by blocking the RAGE/ligand axis.

Next, we conducted experiments to demonstrate the potential of longistatin in extinguishing RAGE-driven proinflammatory activation of cells. Using stimulated HUVEC–based ex vivo experiments, we have directly shown that longistatin ligated with membrane-spanning RAGE, attenuated ROS production, and prevented downstream nuclear translocation of proinflammatory NF-κB. A key consequence of the interaction of ligands (e.g., AGEs, S100 proteins) with RAGE is the generation of ROS, which enhance the nuclear translocation of NF-κB and eventually activate cells (27). Depending on the nature of the pathology, RAGE engagement with its ligand(s) causes activation of multiple intracellular signaling molecules, including the transcription factor NF-κB. In fact, RAGE is a potent inducer of proinflammatory nuclear factor NF-κB (37), and RAGE-dependent activation of NF-κB is the major signaling pathway in many inflammatory conditions. After nuclear translocation, NF-κB binds to specific DNA sequences and activates the transcription of NF-κB–regulated target genes, mainly adhesion molecules and proinflammatory cytokines. Most importantly, in addition to nuclear translocation, RAGE engagement perpetuates NF-κB activation by de novo synthesis of NF-κBp65; thus, it produces a constantly growing pool of this proinflammatory transcription factor (12). Interestingly, after being stimulated by its own ligands, RAGE can cause its self expression, since the *Ager* promoter contains 2 NF-κB–binding sites and subsequently maintains autoamplification of the proinflammatory signals (32). Since RAGE is constitutively present at a higher level in skin (14) and ticks cause extensive cutaneous damage

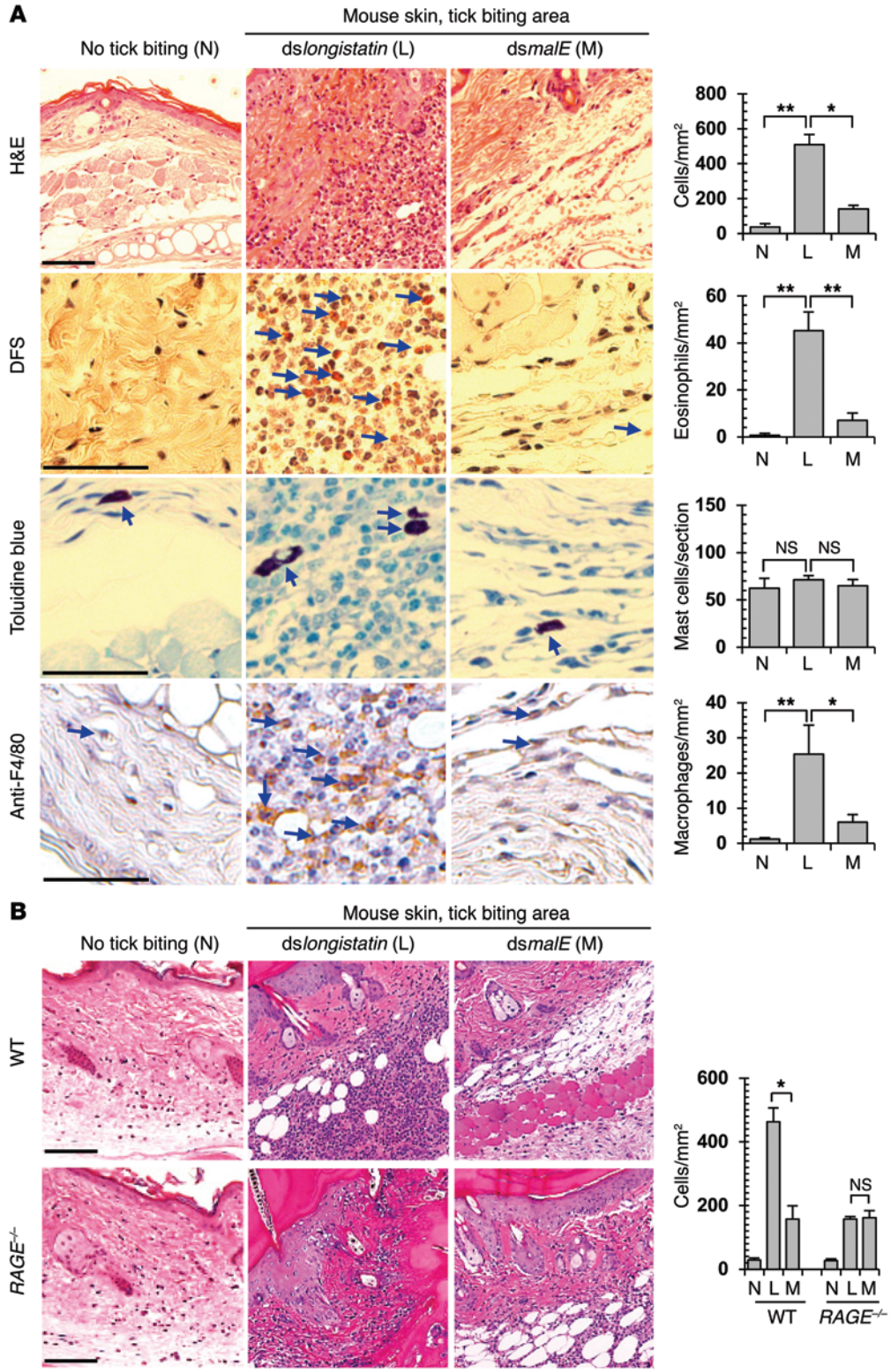

Figure 9. Endogenous longistatin is essential to modulating inflammation during tick feeding. (**A**) Endogenous longistatin suppresses inflammation. We attached RNAi-treated or control ticks to tick-naive WT mice. The mice were sacrificed at day 5 of attachment of the ticks, tissues were collected, and sections were prepared and subjected to H&E or special staining. Then cells were counted. Scale bars: 40 μm. (**B**) Endogenous longistatin suppresses RAGE-mediated inflammation. RNAi-treated or control ticks were allowed to feed on WT or RAGE$^{-/-}$ mice, tissues were collected, and histopathological analysis was performed. Scale bars: 40 μm. $n = 5$. $^{*}P < 0.05$; $^{**}P < 0.01$.

(4, 5), it is quite logical that blockade of RAGE/ligand axis–driven sustained amplification of inflammatory reactions will be beneficial for ticks' feeding success. We also attempted to reveal the consequences of ligation of longistatin with RAGE. We have shown that longistatin efficiently prevented RAGE/ligand-induced upregulation of vascular adhesion molecules, such as VCAM 1, ICAM 1, and eSelectin. These adhesion molecules play essential roles during the recruitment of inflammatory cells into the site of insults (29, 30). We provide data supporting that rlongistatin prevents the secretion of cytokines from endothelial cells induced by RAGE ligands.

Our in vivo inflammation models show that purified rlongistatin significantly suppresses RAGE-mediated inflammation in mam-

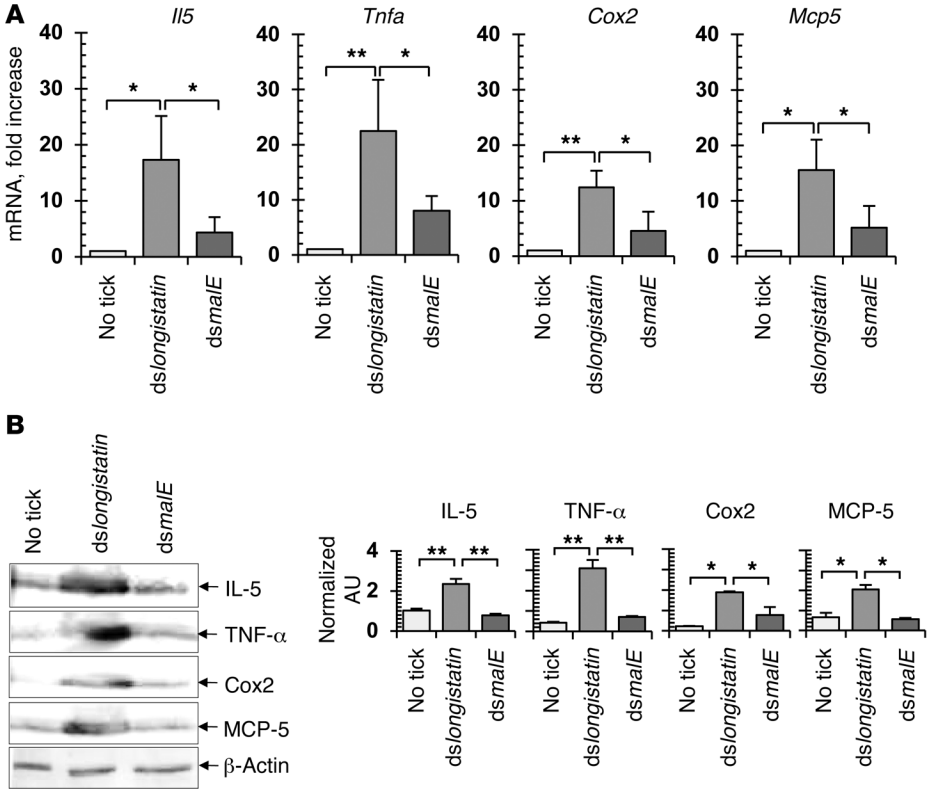

Figure 10. Effect of endogenous longistatin on cytokine production in vivo. RNAi was performed and RNAi-treated or control ticks fed on mice. (**A**) Mouse skin from both control and RNAi groups was collected, and total RNA was isolated. mRNA of cytokines was checked by qRT-PCR. (**B**) Total protein was collected from the mouse tissues and evaluated by WB. Mouse β-actin was used as an internal control. $n = 5$. $^*P < 0.05$; $^{**}P < 0.01$.

mals. Our results conform to the findings of Bierhaus et al. (14), who demonstrated that antagonizing flRAGE with sRAGE can inhibit leukocyte recruitment in a variety of acute and chronic inflammatory conditions. Also, anti-RAGE (e.g., XT-M4 and humanized XT-M4) and low anticoagulant heparin have been shown to interact with the extracellular region of RAGE and inhibit the interactions of RAGE with multiple ligands, thus suppressing inflammation in various experimental models (38). Interestingly, an in vivo tick-feeding model shows that tick biting triggers robust expression of some RAGE ligands at the biting areas of ticks, linking tick-biting pathobiologies with RAGE. In addition to AGE-mediated inflammation suppression by rlongistatin, we clearly showed, using the specific gene-knockdown technique, that endogenous longistatin can also efficiently modulate the infiltration of inflammatory cells at the biting sites of ticks in hosts. More specifically, endogenous longistatin significantly inhibited the infiltration of eosinophils. Eosinophils, the Trojan horses against parasites, play crucial roles in the rejection of ticks in resistant hosts; for example, guinea pigs sensitized to tick feeding express immune resistance to challenge infestations, and this state is associated with the large accumulation of eosinophils around embedded mouth parts (39). Increased eosinophilia has also been detected in the peripheral blood of mice infested with *H. longicornis* larvae (40). Besides the case of tick infestation, there is a marked increase of eosinophils in animals and humans suffering from helminth infections, such as schistosomiasis, ascaridiasis, and trichinellosis. And eosinophils that have increased due to parasitic infections are considered to have an exclusive protective role against parasites (40, 41). Furthermore, we also detected significant modulation of the migration of macrophages by longistatin. Since ticks feed for a long time, the tissue damage is somewhat similar to that seen in chronic inflammation. Possibly, longistatin helps to ensure tick feeding by preventing macrophage migration as well. Findings from an in vivo study using $RAGE^{-/-}$ mice confirm that endogenous longistatin ameliorates RAGE-mediated inflammation during tick feeding.

We provide evidence that endogenous longistatin significantly reduces *Il5*, *Tnfa*, *Cox2*, and *Mcp5* production in hosts during the acquisition of blood meals by ticks. These cytokines play crucial roles in the activation, recruitment, and functions of immune cells. IL-5, known as eosinophil CSF, is a major regulator of eosinophil accumulation in tissues. It critically modulates eosinophil behavior at every stage, from maturation to survival. IL-5 has been shown to have links with asthma and different parasitic diseases (41). On the other hand, TNF-α is chiefly produced by activated macrophages and regulates immune cells. TNF-α, an endogenous pyrogen, can induce fever, and a local increase of its concentration causes cardinal signs of inflammation. Several inhibitors (e.g., Salp15, Iris, and OmC_2) as well as nonprotein molecules (e.g., purine nucleoside adenosine and prostaglandin E_2) isolated from different species of tick have been demonstrated to inhibit TNF-α production (17, 18, 42). And Cox2 is usually expressed at a low level in most tissues, but is significantly upregulated by inflammatory stimuli. It catalyzes the biosynthesis of prostaglandins and has been implicated in the pathogenesis of several inflammatory diseases. RAGE ligands (e.g., endogenous alarmin S100 proteins) have been shown to increase Cox2 expression in RAGE-related inflammatory settings (43). In parasitic diseases, COX2 has also been shown to be upregulated and predicted to have an impact (44). On the other hand, MCP-5, known as an MCP-1–related chemokine, specifically attracts monocytes and eosinophils. Its expression can be dramatically induced in macrophages and plays vital roles in coordinating cellular movement in infections and allergies (45). Although our study clearly shows the mechanistic effects of longistatin on the innate immune system of mammalian hosts, the aa residues of longistatin and RAGE involved in the interaction are yet to be revealed. However, our research is in progress to determine the residues playing key roles. Taken together, our results clearly suggest that longistatin acts as an antagonist to RAGE and suppresses inflammation dur-

ing severe tissue injury induced by biting of ticks; thus, longistatin helps in successful feeding on blood from affected hosts.

Methods

Ticks. We propagated and maintained colonies of the parthenogenetic Okayama strain of *H. longicornis* at the Laboratory of Parasitic Diseases, NIAH, by feeding on the ear of tick-naive, specific-pathogen free (SPF) Japanese white rabbits (20).

Animals and generation of RAGE-null mice. RAGE$^{-/-}$ mice were produced and maintained as previously described (46). All animals used in this study were acclimatized to the experimental conditions for 2 weeks prior to the commencement of the experiment.

rlongistatin. rlongistatin was produced and purified as described (47). His-tag was removed from longistatin by incubating with enterokinase (EKMax; Invitrogen) and purifying (Ek-Away Resin; Invitrogen). Endotoxin was removed using ProteoSpin Endotoxin Removal Micro Kit (Norgen). Metal contaminants were removed by dialyzing longistatin against 10 mM EDTA.

Anti-longistatin. Ab against longistatin was generated in BALB/c mice by injecting longistatin (30 μg/mouse) emulsified with TiterMax Gold adjuvant (Sigma-Aldrich), followed by a booster immunization 2 weeks apart (47).

AGE production. AGE-BSA was produced by incubating BSA (10 mg) with DL-glyceraldehyde (100 mg) in 1 ml of 0.2 M phosphate buffer (pH 7.4) at 37°C for 3 days under strict sterile conditions (48). Contaminating LPS, if any, was removed with Acrodisc units fitted with Mustang (Pall Corp.) and extensively dialyzed in PBS. Modification of BSA into Gla-BSA was confirmed by checking the binding ability with RAGE.

Microtiter plate binding assay. RAGE (5 μg/ml; R&D) was coated onto an ELISA plate (Nunc) and washed with TBS-T. After blocking, wells were reacted with longistatin or BSA at different concentrations (0–384 nM) in 50 μl of buffer A (50 mM Tris-HCl, pH 7, 10 mM sodium chloride, 5 mM calcium chloride) for 1 hour at room temperature (RT). After washing, anti-longistatin (1:1000) or anti-BSA (1:1000, Sigma-Aldrich) was added, followed by HRP-conjugated IgG for 1 hour at RT. Reactions were developed with TMB One Solution (Promega) and read at 450 nm (OD_{450}). In a RAGE-dependent study, wells were coated with longistatin (4 μg/ml) and treated with RAGE or TLR4 (R&D) at different concentrations (0–5 μg/ml) in buffer A. Bound proteins were detected with anti-RAGE (1:500, Millipore) or anti-TLR4 (1:500, Proteintech). Additionally, to compare the binding ability of longistatin with that of other RAGE ligands, an equal amount (5 μg/ml) of longistatin or each of other ligands, such as CML-BSA (CycLex Co.), Gla-BSA, HMGB1 (Abnova), or S100A12 (Abnova) was coated onto ELISA plates. After blocking, RAGE (2 μg/ml) was added and binding was detected with anti-RAGE (1:500). For Ca^{2+}-dependent RAGE binding, RAGE-coated (5 μg/ml) wells were treated with longistatin or metal-free longistatin (6 μg/ml) in buffer A with or without 5 mM calcium chloride, respectively, and binding of longistatin was determined. For binding inhibition, either longistatin was preincubated with anti-longistatin or bound RAGE was reacted with anti-RAGE. Furthermore, amounts of longistatin bound to RAGE were estimated using longistatin standard curve, and K_D value was calculated by Scatchard plot (4).

Competitive binding. RAGE (4 μg/ml) was coated onto ELISA plate and blocked. Then wells were treated with longistatin alone or with the mixture of longistatin (1 μg/ml) and each of other RAGE ligands (5 μg/ml), such as S100A12, S100A6 (Sino Biological Inc.), HMGB1, CML-BSA, or Gla-BSA, in buffer A for 1 hour at RT. After extensive washing, bound longistatin was detected with anti-longistatin.

Domain assay. Genes encoding RAGE domain V, C1, and C2 were ligated into pTrcHisB (Takara) and expressed in *E. coli*. Single domains were purified; His-tag was removed and dialyzed as described (47). Purified recombinant V, C1, or C2 domain was coated onto an ELISA plate and reacted with longistatin; bound longistatin was detected.

Homology modeling and docking. 3D homology models of longistatin and the V domain of RAGE were derived from the Swiss model (36.0003) program (49). Model structures of longistatin and the V domain of RAGE were built using hMCFD2 (PDB 2VRGA) and hRAGE (PDB 3O3U) as respective templates. The structures were visualized with PyMOL (The PyMOL Molecular Graphics System, version 1.1; Schrödinger LLC). Computational docking of longistatin to the V domain of RAGE was performed using ClusPro 2.0 (50).

HUVEC culture, treatment, stimulation, and subcellular fractionation. HUVECs (2.5×10^5) were cultured in T_{25} cell culture flasks in a growth medium (Cell Application Inc.) as described (51), and were treated with endotoxin-free longistatin (10 μg/ml) for 12 hours and then stimulated with Gla-BSA (100 μg/ml) or TNF-α (1 ng/ml; Wako) for a further 12 hours. As a control, cells were left untreated without stimulation or stimulated with Gla-BSA (100 μg/ml) or TNF-α (1 ng/ml) without prior longistatin treatment. Subcellular fractions were collected using ProteoExtract Subcellular Proteome Extraction Kit (Calbiochem). Whole-cell lysate was collected as described (52).

HUVECs fraction binding assays. Longistatin (5 μg/ml) was coated onto an ELISA plate and blocked. Wells were treated with TNF-α–stimulated (1 ng/ml) HUVEC whole-cell lysate (20 μg) in buffer A for 1 hour at RT. Bound RAGE-specific antigen was detected with anti-RAGE (1:1600 to 1:100). Additionally, HUVEC whole-cell lysate (20 μg) was coated onto an ELISA plate and treated with sheep anti-sRAGE at various concentrations (0 to 1:100). After washing, longistatin was added to the wells and incubated further for 1 hour at RT. Bound longistatin was probed with anti-longistatin (1:1000). Furthermore, equal amounts of different subcellular fractions (20 μg/ml) were coated onto ELISA plates. After blocking, longistatin (4 μg/ml) was added and incubated for 1 hour at RT and bound longistatin was detected.

Colocalization. HUVECs were grown on chamber slides (Nunc), serum starved, and stimulated with TNF-α (1 ng/ml) for 12 hours. Cells were fixed with 4% paraformaldehyde, blocked with 1% BSA, and treated with longistatin (5 μg/ml, in buffer A) for 12 hours at 4°C. After washing, cells were treated with anti-longistatin (1:1000) and anti-RAGE (1:1000). Bound antibodies were detected using green fluorescent–labeled (Alexa Fluor 488 goat anti-mouse IgG [H+L]; Invitrogen) and red fluorescent–labeled (Alexa Fluor 594 goat anti-rabbit IgG [H+L]; Invitrogen) IgG. Slides were mounted with DAPI and photographed (Leica Microsystems), and images were merged.

Pull-down assay. His-tagged longistatin (10 μg) was trapped with Talon Metal Affinity Resin (Clontech Laboratories Inc.) as described (53) and incubated with the membrane fraction (100 μg) of stimulated HUVECs in buffer A. After washing, proteins were eluted and separated by 12.5% SDS-PAGE under reducing conditions and transferred onto a nitrocellulose membrane. WB was performed using anti-longistatin (1:1000) or anti-RAGE (1:1000) (4).

siRNA. RAGE siRNA duplex and a nonspecific negative control siRNA were purchased (Bioneer). HUVECs were transfected with

siRNA using Lipofectamine RNAiMAX Reagent (Life Technologies) following the manufacturer's instructions.

Ex vivo cell attachment assay. Ninety-six–well cell-culture plates were coated with BSA, longistatin, or CML-BSA (5 μg/ml) and blocked. After washing, wells were treated without or with sRAGE (5 μg/ml) for 1 hour at RT. Then TNF-α–stimulated (1 ng/ml) HUVECs (2×10^3 cells/well) were seeded and incubated for 2 hours in a humidified incubator in the presence of 5% CO_2. Plates were washed gently in PBS, and adhered cells were counted. We also conducted cell-attachment assays using siRNA-treated cells.

ROS inhibition. HUVECs (1×10^5 cells/chamber) were seeded onto chamber slides or black-sided 96-well cell-culture plates and allowed to adhere overnight. Cells were treated without or with Gla-BSA (100 μg/ml) in the absence or presence of pretreatment with anti-RAGE (1:100), DPI (20 μM), MITO-tempo (10 μM), or longistatin (10 μg/ml) for 2 hours at 37°C. Cellular ROS were detected with the DCFDA Cellular ROS Detection Kit following the manufacturer's instructions (Abcam).

NF-κB translocation inhibition. HUVECs were grown on chamber slides. Cells were serum starved and treated without or with longistatin (10 μg/ml) or anti-RAGE (1:100) for 12 hours at 37°C and then stimulated without or with Gla-BSA (100 μg/ml) for a further 12 hours under the same conditions. Cells were fixed with 4% paraformaldehyde and permeabilized with 0.1% Triton X-100. After blocking, cells were treated with anti–NF-κB (1:1000) overnight at 4°C. Bound antibodies were detected using green fluorescent–labeled IgG. In addition, HUVECs were cultured in T_{25} flasks and treated with longistatin (0–10 μg/ml) or anti-RAGE (1:100) and stimulated up to different time points (0–12 hours). Cytoplasmic and nuclear fractions were separated in complete protease and phosphatase inhibitors (52). An equal amount of each fraction (50 μg/ml) was coated onto the wells of an ELISA plate. After blocking, wells were treated with anti–NF-κB (1:1000), and bound Ab was detected using an HRP-conjugated IgG. Furthermore, we detected NF-κB in the cytosolic and nuclear fraction by WB. Additionally, equal amounts (30 μg) of cytosolic protein from different treatment groups were separated by SDS-PAGE, and WB was performed using antibodies against IκB-α, phospho–IκB-α, and β-actin.

qRT-PCR. HUVECs were cultured, treated with longistatin or anti-RAGE (1:100), and stimulated with Gla-BSA, and total RNA was collected (4). Expression patterns of *VCAM1*, *ICAM1*, and E-selectin (primers in Supplemental Table 1) were checked on a LightCycler 1.5 instrument (Roche Instrument Centre AG) using LightCycler Fast-Start DNA Master SYBR Green I (Roche Diagnostics). β-Actin was used to normalize the amount of cDNA (54), and data were analyzed using LightCycler Software version 3.5.

Cytokines. HUVECs were cultured and stimulated as above, medium was collected, and cytokines were measured using the Multi-Analyte ELISArray kit (QIAGEN).

Chemotaxis inhibition. mPRCs were collected from WT and $RAGE^{-/-}$ mice and treated without or with longistatin (2.5–10 μg/ml) or anti-RAGE (1:100) for 30 minutes at 37°C or left untreated. Cells were applied onto the upper chamber of 24-well–type Chemotaxicell (8 μm pore, polycarbonate membrane) in RPMI-1640 medium. The lower chamber contained RPMI-1640 medium with Gla-BSA (0–100 μg/ml) and was incubated at 37°C for 4 hours. After gentle washing, membrane was stained with Giemsa stain, and cells were counted under a ×40 objective.

Footpad inflammation model. Longistatin (100 μg) or PBS was injected into the hind footpad of each WT or $RAGE^{-/-}$ mouse. One hour later, 2% carrageenan or saline (100 μl) was injected into the same footpad. As a positive control, only 2% carrageenan (100 μl) was injected. Saline-alone–injected footpad served as a negative control. After 5 hours, mice were euthanized and footpads were collected and fixed in 4% paraformaldehyde for 48 hours at 4°C. Samples were decalcified, and thin (5 μm) sections were prepared and stained with H&E. We counted inflammatory cells manually in 3 fields under a ×40 objective in each of the 3 sections from each mouse using a 100-square (1 mm × 1 mm) grid. To study the effects of longistatin on RAGE/ligand axis–mediated inflammation, longistatin (100 μg) or PBS was injected into the hind footpad of each mouse. One hour later, Gla-BSA (100 μg) was injected into the same footpad. As a positive control, only Gla-BSA (100 μg) was injected. PBS-alone–injected footpad served as a negative control. After 8 hours, mice were euthanized, and footpads were collected and analyzed.

Pneumonia model. Longistatin (50 μg) or PBS was instilled through each nostril of WT mice. One hour later, Gla-BSA (50 μg) or PBS was instilled. After 48 hours, mice were euthanized and lungs were collected and fixed for 24 hours. Sections were prepared and stained, and inflammatory cells were counted.

RNAi, histopathology, immunohistochemistry, and cytokine profiling. We synthesized dsRNA complementary to longistatin or *E. coli malE* gene, and performed RNAi by injecting 1 μg of longistatin dsRNA (dslongistatin, treated group) or ds*malE* (control group) into each unfed adult tick (4). We attached RNAi-treated or control ticks or normal ticks (without any treatment) on the shaven backs of tick-naive WT or $RAGE^{-/-}$ mice (47). Mice were euthanized at day 5 of attachment of the ticks or at different time points (0–120 hours), and tissues were collected from the feeding lesions or from the selected areas. Sections were prepared and stained with H&E, DFS, or toluidine blue. We also performed immunohistochemistry using antibodies against F4/80 (0.5 μg/ml; BMA Biomedicals), myeloperoxidase (25 μg/ml; R&D), CD3 (1:50; Santa Cruz Biotechnology Inc.), CD4 (25 μg/ml; R&D), CD8 (25 μg/ml; R&D), CD20 (1:50; Santa Cruz Biotechnology Inc.), or CD117 (1:50, BioLegend Inc.) as described (20) as well as counterstaining with hematoxylin; cells were counted. Additionally, total RNA was collected from mouse skin from both RNAi-treated and control groups, and *Il5*, *Tnfa*, *Cox2*, and *Mcp5* were checked by qRT-PCR. We also analyzed the expression pattern of RAGE and some RAGE ligands at the biting areas of normal ticks at different feeding phases (0–120 hours) by qRT-PCR. Furthermore, we collected tissues from the attachment sites of ticks, and total protein was harvested and analyzed by WB using antibodies against IL-5, TNF-α, COX2, MCP-5, or β-actin.

Statistics. Data are presented as mean ± SEM. For multiple group comparisons, 1-way ANOVA followed by post-hoc Bonferroni's analysis was used. For direct comparisons, unpaired 2-tailed Student's *t* test was employed. A value of $P < 0.05$ was considered as significant.

Study approval. This study was carried out in strict accordance with the recommendations in the Guide for the Care and Use of Laboratory Animals of the NIAH. The protocol was approved by the Committee of the Ethics of Animal Experiments of the NIAH (permit numbers: *09-017*, *09-018*, *10-008*, *10-010*, *11-027*, *A-13-028*). All surgeries were performed under sodium pentobarbital anesthesia, and all efforts were made to minimize the animals' suffering.

Acknowledgments

This work was supported by a postdoctoral fellowship for foreign researchers (to Anisuzzaman) provided by the Japan Society for the Promotion of Science (JSPS). It was also supported by Grants-in-Aid (to N. Tsuji) from the Ministry of Education, Culture, Sports, Science and Technology of Japan and a grant (to N. Tsuji) for Promotion of Basic Research Activities for Innovative Biosciences from the Bio-oriented Technology Research Advancement Institution. We are grateful to K. Kita and M. Shafiqul Islam of The University of Tokyo for helpful discussion. We thank M. Shimada and M. Kobayashi for their generous help in preparing histological sections.

Address correspondence to: Naotoshi Tsuji, Laboratory of Parasitic Diseases, NIAH, National Agricultural and Food Research Organization, 3-1-5 Kannondai, Tsukuba, Ibaraki 305-0856, Japan. Phone: 81.29.838.7749; E-mail: tsujin@affrc.go.jp.

1. Fujisaki K, Kawaju S, Kamio T. The taxonomy of the bovine Theileria spp. *Parasitol Today*. 1994;10(1):31–33.
2. Murray TS, Shapiro ED. Lyme disease. *Clin Lab Med*. 2010;30(1):311–328.
3. Cui F, et al. Clinical and epidemiological study on severe fever with thrombocytopenia syndrome in Yiyuan County, Shandong Province, China. *Am J Trop Med Hyg*. 2013;88(3):510–512.
4. Anisuzzaman, et al. Longistatin, a plasminogen activator, is key to the availability of blood-meals for ixodid ticks. *PLoS Pathog*. 2011;7(3):e1001312.
5. Sonenshine DE. *Biology Of Ticks*. Vol 1, New York, New York, USA: Oxford University Press; 1991.
6. Chen GY, Nuñez G. Sterile inflammation: sensing and reacting to damage. *Nat Rev Immunol*. 2010;10(12):826–837.
7. van Zoelen MA, Achouiti A, van der Poll T. The role of receptor for advanced glycation endproducts (RAGE) in infection. *Crit Care*. 2011;15(2):208.
8. Janeway CA Jr, Medzhitov R. Innate immune recognition. *Annu Rev Immunol*. 2002;20:197–216.
9. Bianchi ME, et al. DAMPs, PAMPs and alarmins: all we need to know about danger. *J Leukoc Biol*. 2007;81(1):1–5.
10. Schmidt AM, Yan SD, Yan SF, Stern DM. The multiligand receptor RAGE as a progression factor amplifying immune and inflammatory responses. *J Clin Invest*. 2001;108(7):949–955.
11. González I, Romero J, Rodríguez BL, Pérez-Castro R, Rojas A. The immunobiology of the receptor of advanced glycation end-products: trends and challenges. *Immunobiology*. 2013;218(5):790–797.
12. Sparvero LJ, et al. RAGE (receptor for advanced glycation endproducts), RAGE ligands, and their role in cancer and inflammation. *J Transl Med*. 2009;7:17.
13. Chavakis T, et al. The pattern recognition receptor (RAGE) is a counterreceptor for leukocyte integrins: a novel pathway for inflammatory cell recruitment. *J Exp Med*. 2003;198(10):1507–1515.
14. Bierhaus A, et al. Understanding RAGE, the receptor for advanced glycation end products. *J Mol Med*. 2005;83(11):876–886.
15. Chavakis T, Bierhaus A, Nawroth PP. RAGE (receptor for advanced glycation end products): a central player in the inflammatory response. *Microbes Infect*. 2004;6(13):1219–1225.
16. Moser B, et al. Receptor for advanced glycation end products expression on T cells contributes to antigen-specific cellular expansion in vivo. *J Immunol*. 2007;179(12):8051–8058.
17. Koník P, Slavíková V, Salát J, Reznícková J, Dvoroznáková E, Kopecký J. Anti-tumour necrosis factor-α activity in Ixodes ricinus saliva. *Parasite Immunol*. 2006;28(12):649–656.
18. Hovius JW, Levi M, Fikrig E. Salivating for knowledge: potential pharmacological agents in tick saliva. *PLoS Med*. 2008;5(2):e43.
19. Kopácek P, Hajdusek O, Buresová V, Daffre S. Tick innate immunity. *Adv Exp Med Biol*. 2011;708:137–162.
20. Anisuzzaman, et al. Longistatin, a novel EF-hand protein from the ixodid tick Haemaphysalis longicornis, is required for acquisition of host blood-meals. *Int J Parasitol*. 2010;40(6):721–729.
21. Anisuzzaman, et al. Longistatin, a novel plasminogen activator from vector ticks, is resistant to plasminogen activator inhibitor-1. *Biochem Biophys Res Commun*. 2011;413(4):599–604.
22. Leclerc E, Fritz G, Vetter SW, Heizmann CW. Binding of S100 proteins to RAGE: an update. *Biochim Biophys Acta*. 2009;1793(6):993–1007.
23. Leclerc E, Heizmann CW. The importance of Ca^{2+}/Zn^{2+} signaling S100 proteins and RAGE in translational medicine. *Front Biosci (Schol Ed)*. 2011;3:1232–1262.
24. Rao NV, et al. Low anticoagulant heparin targets multiple sites of inflammation, suppresses heparin-induced thrombocytopenia, and inhibits interaction of RAGE with its ligands. *Am J Physiol Cell Physiol*. 2010; 299(1):C97–C110.
25. Ramasamy R, Yan SF, Schmidt AM. Receptor for AGE (RAGE): signaling mechanisms in the pathogenesis of diabetes and its complications. *Ann N Y Acad Sci*. 2011;1243:88–102.
26. Maillard-Lefebvre H, Boulanger E, Daroux M, Gaxatte C, Hudson BI, Lambert M. Soluble receptor for advanced glycation end products: a new biomarker in diagnosis and prognosis of chronic inflammatory diseases. *Rheumatology*. 2009;48(10):1190–1196.
27. Wautier MP, Chappey O, Corda S, Stern DM, Schmidt AM, Wautier JL. Activation of NADPH oxidase by AGE links oxidant stress to altered gene expression via RAGE. *Am J Physiol Endocrinol Metab*. 2001;280(5):E685–E694.
28. Mahali S, Raviprakash N, Raghavendra PB, Manna SK. Advanced glycation end products (AGEs) induce apoptosis via a novel pathway: involvement of Ca^{2+} mediated by interleukin-8 protein. *J Biol Chem*. 2011;286(40):34903–34913.
29. Mori S, et al. Ciprofloxacin inhibits advanced glycation end products-induced adhesion molecule expression on human monocytes. *Br J Pharmacol*. 2010;161(1):229–240.
30. Li H, et al. ROCK inhibitor fasudil attenuated high glucose-induced MCP-1 and VCAM-1 expression and monocyte-endothelial cell adhesion. *Cardiovasc Diabetol*. 2012;11:65.
31. Lohwasser C, Neureiter D, Weigle B, Kirchner T, Schuppan D. The receptor for advanced glycation end products is highly expressed in the skin and upregulated by advanced glycation end products and tumor necrosis factor-α. *J Invest Dermatol*. 2006;126(2):291–299.
32. Lange-Sperandio B, Sperandio M, Nawroth P, Bierhaus A. RAGE signaling in cell adhesion and inflammation. *Curr Pediatr Rev*. 2007;3(1):1–9.
33. Ma W, Rai V, Hudson BI, Song F, Schmidt AM, Barile GR. RAGE binds C1q and enhances C1q-mediated phagocytosis. *Cell Immunol*. 2012;274(1–2):72–82.
34. Ruan BH, et al. Complement C3a, CpG oligos, and DNA/C3a complex stimulate IFN-α production in a receptor for advanced glycation end product-dependent manner. *J Immunol*. 2010;185(7):4213–4222.
35. Yan SD, et al. RAGE and amyloid-beta peptide neurotoxicity in Alzheimer's disease. *Nature*. 1996;382(6593):685–691.
36. Prevot PP, et al. Anti-hemostatic effects of a serpin from the saliva of the tick Ixodes ricinus. *J Biol Chem*. 2006;281(36):26361–26369.
37. Gebhardt C, et al. RAGE signaling sustains inflammation and promotes tumor development. *J Exp Med*. 2008;205(2):275–285.
38. Vugmeyster Y, DeFranco D, Pittman DD, Xu X. Pharmacokinetics and lung distribution of a humanized anti-RAGE antibody in wild-type and $RAGE^{-/-}$ mice. *MAbs*. 2010;2(5):571–575.
39. Brown SJ, Askenase PW. Blood eosinophil and basophil responses in guinea pigs parasitized by Amblyomma americanum ticks. *Am J Trop Med Hyg*. 1982;31(3):593–598.
40. Ushio H, et al. Mechanisms of eosinophilia in mice infested with larval Haemaphysalis longicornis ticks. *Immunology*. 1995;84(3):469–475.
41. Masure D, et al. A role for eosinophils in the intestinal immunity against infective Ascaris suum larvae. *PLoS Negl Trop Dis*. 2013;7(3):e2138.
42. Oliveira CJ, et al. Deconstructing tick saliva: non-protein molecules with potent immunomodulatory properties. *J Biol Chem*. 2011;286(13):10960–10969.
43. Shanmugam N, Kim YS, Lanting L, Natarajan R. Regulation of cyclooxygenase-2 expression in monocytes by ligation of the receptor for advanced glycation end products. *J Biol Chem*. 2003;278(37):34834–34844.
44. Corral RS, Guerrero NA, Cuervo H, Gironès N, Fresno M. Trypanosoma cruzi infection and endothelin-1 cooperatively activate pathogenic inflammatory pathways in cardiomyocytes. *PLoS Negl Trop Dis*. 2013;7(2):e2034.
45. Sarafi MN, Garcia-Zepeda EA, MacLean JA, Charo IF, Luster AD. Murine monocyte chemoat-

tractant protein (MCP)-5: a novel CC chemokine that is a structural and functional homologue of human MCP-1. *J Exp Med*. 1997;185(1):99–109.
46. Myint KM, et al. RAGE control of diabetic nephropathy in a mouse model: effects of RAGE gene disruption and administration of low-molecular weight heparin. *Diabetes*. 2006;55(9):2510–2522.
47. Anisuzzaman, et al. Longistatin is an unconventional serine protease and induces protective immunity against tick infestation. *Mol Biochem Parasitol*. 2012;182(1–2):45–53.
48. Takeuchi M, et al. Immunological detection of a novel advanced glycation end-product. *Mol Med*. 2001;7(11):783–791.
49. Schwede T, Kopp J, Guex N, Peitsch MC. SWISS-MODEL: An automated protein homology-modeling server. *Nucleic Acids Res*. 2003;31(13):3381–3385.
50. Comeau SR, Gatchell DW, Vajda S, Camacho CJ. ClusPro: an automated docking and discrimination method for the prediction of protein complexes. *Bioinformatics*. 2004;20(1):45–50.
51. Islam MK, et al. The Kunitz-like modulatory protein haemangin is vital for hard tick blood-feeding success. *PLoS Pathog*. 2009;5(7):e1000497.
52. Shimazu R, et al. MD-2, a molecule that confers lipopolysaccharide responsiveness on Toll-like receptor 4. *J Exp Med*. 1999;189(11):1777–1782.
53. Anisuzzaman, Islam MK, Alim MA, Tsuji N. Longistatin, an EF-hand Ca^{2+}-binding protein from vector tick: identification, purification, and characterization. In: Heizmann CW, ed. *Calcium-Binding Proteins and RAGE: From Structural Basics to Clinical Applications, Methods in Molecular Biology*. Vol. 963. New York, New York, USA: Humana Press; 2013:127–146.
54. Chen Y, et al. RAGE ligation affects T cell activation and controls T cell differentiation. *J Immunol*. 2008;181(6):4272–4278.